NRL Memorandum Report 5053

Numerical Simulation of the Axisymmetric Hollowing Instability

G. JOYCE AND M. LAMPE

Plasma Theory Branch
Plasma Physics Division

April 14, 1983

This work was supported by Defense Advanced Research Projects Agency under ARPA Order 4395, Amendment No. 1, monitored by Naval Surface Weapons Center under N60921-82-WR-W0066.

NAVAL RESEARCH LABORATORY
Washington, D.C.

SECURITY CLASSIFICATION OF THIS PAGE (When Data Entered)

REPORT DOCUMENTATION PAGE	READ INSTRUCTIONS BEFORE COMPLETING FORM
1. REPORT NUMBER: NRL Memorandum Report 5053 — 2. GOVT ACCESSION NO.	3. RECIPIENT'S CATALOG NUMBER
4. TITLE (and Subtitle): NUMERICAL SIMULATION OF THE AXISYMMETRIC HOLLOWING INSTABILITY	5. TYPE OF REPORT & PERIOD COVERED: Interim report on a continuing NRL problem.
	6. PERFORMING ORG. REPORT NUMBER
7. AUTHOR(s): G. Joyce and M. Lampe	8. CONTRACT OR GRANT NUMBER(s)
9. PERFORMING ORGANIZATION NAME AND ADDRESS: Naval Research Laboratory, Washington, DC 20375	10. PROGRAM ELEMENT, PROJECT, TASK AREA & WORK UNIT NUMBERS: 47-0900-0-2
11. CONTROLLING OFFICE NAME AND ADDRESS: Defense Advanced Research Projects Agency, Arlington, VA 22209	12. REPORT DATE: April 14, 1983
	13. NUMBER OF PAGES: 41
14. MONITORING AGENCY NAME & ADDRESS(if different from Controlling Office): Naval Surface Weapons Center Detachment, Silver Spring, MD 20910	15. SECURITY CLASS. (of this report): UNCLASSIFIED
	15a. DECLASSIFICATION/DOWNGRADING SCHEDULE

16. DISTRIBUTION STATEMENT (of this Report)

Approved for public release; distribution unlimited.

17. DISTRIBUTION STATEMENT (of the abstract entered in Block 20, if different from Report)

18. SUPPLEMENTARY NOTES

This work was supported by Defense Advanced Research Projects Agency under ARPA Order 4395, Amendment No. 1, monitored by Naval Surface Weapons Center under N60921-82-WR-W0066.

19. KEY WORDS (Continue on reverse side if necessary and identify by block number)

Beam propagation
Relativistic electron beams
Sausage instability
Hollowing instability
Beam instabilities
Charged particle beams
Axisymmetric instability of beams

20. ABSTRACT (Continue on reverse side if necessary and identify by block number)

Recent simulations have indicated that highly current-neutralized charged particle beams propagating in an ionizable gas are subject to violent axisymmetric instabilities. We show that these instabilities are excitations of the m = 0, n = 2 hollowing mode, for which there is no adequate analytic theory. We present results of a wide-ranging simulation study of the instability mechanism and the parameter range of the instability.

DD FORM 1 JAN 73 1473 EDITION OF 1 NOV 65 IS OBSOLETE
S/N 0102-014-6601

SECURITY CLASSIFICATION OF THIS PAGE (When Data Entered)

Table of Contents

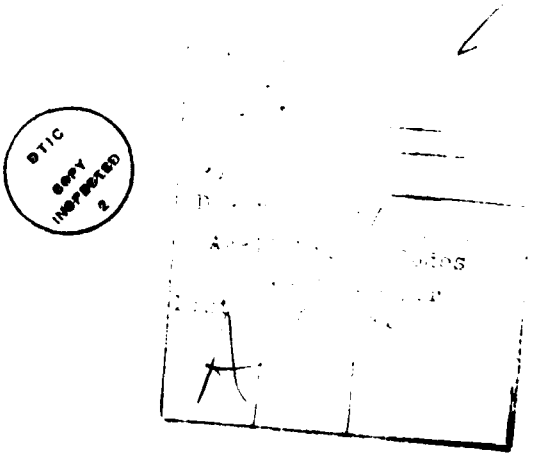

NUMERICAL SIMULATION OF THE AXISYMMETRIC HOLLOWING INSTABILITY

1. Introduction

Because of the rapid ionization of the gas in the vicinity of the beam head, a self-pinched electron beam may experience a large degree of current neutralization.[1] The repulsive forces between the beam and return current lead to a number of instabilities, many of which have been studied in the literature on beam propagation in high temperature plasmas.[2-7] The axisymmetric modes, while stable when the plasma current is small, can be driven unstable when the plasma current is a large fraction of the beam current. In a companion paper[8], we have shown that the inclusion of self-consistent beam-driven ionization stabilizes the sausage mode for a beam propagating into an initially unionized gas. Several numerical simulations, however, have shown the existence of axisymmetric instabilities in a significant range of beam currents and gas density.[9-11] We show in this paper that those instabilities are not excitations of the sausage mode but of the m = 0, n = 2 hollowing mode.[12] Because there is no fully adequate analytic theory for the hollowing mode, we have pursued a wide ranging simulation study with two objectives: The first is to elucidate the destabilizing mechanism. The second is to determine quantitatively the parameter range in which the instability is expected. The instability turns out to be a subtle one requiring large return current, strong avalanche ionization, and peaking of the avalanche on axis. An outline of the paper is as follows: Section 2 is a discussion of the simulation code; Section 3 presents the general features of the instability in a uniform gas; Section 4 shows the importance of avalanche as the destabilizing mechanism; Section 5 presents the dependence of

Manuscript approved January 28, 1983.

the instability on beam parameters; Section 6 discusses improvements which may be made in the conductivity model; Section 7 suggests a method of stabilizing the mode; Section 8 discusses the status of experiments; and Section 9 presents the conclusions.

2. SIMMO

The particle simulation code SIMMO (pronounced simm-zero) is an axially symmetric "ring-in-cell" code in which a large number of charged rings are followed in time as they interact with each other through the fields generated by the particles themselves and by the background gas ionized by the beam. We use the reduced set of Maxwell's equations derived by Lee[13] employing the paraxial approximation and Doppler shifted coordinates. We neglect terms of the order r/λ_β where r is a radial scale length and λ_β is the betatron wavelength. We also neglect terms of order γ^{-2} where γ is the relativistic factor. We use as our independent variables z and $\zeta = ct - z$ where t is the time and ct is the position of the beam head in space. The coordinate ζ is a measure of the distance along the axis from the beam head. With these approximations we can write Maxwell's equations in the Lorentz gauge as

$$\nabla_\perp^2 \vec{A}_\perp = -\frac{4\pi}{c} \vec{J}_\perp \tag{1}$$

$$\nabla_\perp^2 A_z = -\frac{4\pi}{c} J_z \tag{2}$$

$$\nabla_\perp^2 \phi = -4\pi\rho \tag{3}$$

$$\nabla_\perp \cdot \vec{J}_\perp - \frac{\partial J_z}{\partial \zeta} + \frac{\partial c\rho}{\partial \zeta} = 0 \tag{4}$$

$$\nabla_\perp \cdot \vec{A}_\perp - \frac{\partial A_z}{\partial \zeta} + \frac{\partial \phi}{\partial \zeta} = 0 \tag{5}$$

where $\vec{A}$ is the vector potential, ϕ is the scalar potential, the subscript z is associated with the axial direction and the subscript $\perp$ is associated with the radial variables r and θ.

The electromagnetic fields can be obtained from the potentials from the relations:

$$\vec{E}_\perp = -\frac{\partial \vec{A}_\perp}{\partial \zeta} - \nabla_\perp \phi \tag{6}$$

$$E_z = -\frac{\partial A_z}{\partial \zeta} + \frac{\partial \phi}{\partial \zeta} \tag{7}$$

$$\vec{B}_\perp = -\hat{e}_z \times \left(\nabla_\perp A_z + \frac{\partial \vec{A}_\perp}{\partial \zeta}\right) \tag{8}$$

$$B_z = \left[\nabla_\perp \times \vec{A}\right]_z \tag{9}$$

and the current densities are given by

$$\vec{J}_\perp = \sigma \vec{E}_\perp \tag{10}$$

$$J_z = J_{bz} + \sigma E_z \tag{11}$$

where σ is the scalar conductivity and J_{bz} is the beam current density. Because of the paraxial approximation, $J_{b\perp}$ can be neglected as a source term in Maxwell's equation.

The dynamical equations are calculated in Cartesian Coordinates from the equations

$$\frac{\partial(\gamma \vec{v}_\perp)}{\partial z} = \frac{q}{mc} \nabla_\perp (A_z - \phi) \tag{12}$$

$$\frac{\partial \gamma}{\partial z} = \frac{-q}{mc^2} \nabla_\perp \cdot \vec{A}_\perp. \tag{13}$$

Because of the ultra-relativistic and paraxial approximations it can be assumed that all beam particles have axial velocity c, so that beam dynamics takes place only in the transverse plane. The fields are known on a regularly spaced grid and are interpolated to the particle positions by a quadratic scheme.

The code determines the conductivity $\sigma(r, \zeta, z)$ from the equation

$$\frac{\partial \sigma}{\partial \zeta} = \kappa J_b + \nu_i \frac{\sigma}{c}, \tag{14}$$

where the first term represents direct ionization by the beam and the second term represents avalanche. We use the value[14]

$$\kappa = \frac{e^2}{m\nu_m} \frac{\partial n_e}{\partial \zeta} \frac{1}{J_b} = 8.48 \times 10^{-4} \text{cm/statcoul}, \tag{15a}$$

corresponding to an effective electron-molecule collision frequency for air

$$\nu_m = 1.414 \times 10^{12} (T_e/1\text{eV})^{1/2} \rho \ \text{sec}^{-1} \tag{15b}$$

with an assumed electron temperature

$$T_e = 2\text{eV}, \tag{15c}$$

and the avalanche ionization coefficient specified for air as[15]

$$\nu_i = \frac{A\rho S^3}{1 + BS + CS^2 + DS^3} \ \text{sec}^{-1}, \tag{16}$$

where

$$S \equiv E^2/\rho^2, \tag{17a}$$

E is the electric field in statvolts/cm, ρ is the air density in atmospheres, and

$$A = 1.42 \times 10^{-4}, \tag{17b}$$

$$B = 9.18 \times 10^{-6}, \tag{17c}$$

$$C = 2.66 \times 10^{-10}, \tag{17d}$$

$$D = 2.82 \times 10^{-17}. \tag{17e}$$

Our usual initial condition is

$$\sigma (r, 0, 0) = 0. \tag{18}$$

The treatment of particle dynamics is well known so we will not dwell on it here. The initial conditions are chosen so that the back end of the beam is in equilibrium with the ionized gas. This is accomplished by choosing the beam particles to have a Maxwellian distribution of perpendicular velocities characterized by a thermal speed

$$v_{th} \propto \frac{I_{eff}}{I_A} c, \tag{19}$$

where I_{eff} is the net current associated with the mean pinch force, and is calculated from the initial conditions, while $I_A \approx 17\beta\gamma$ kA is the Alfven current. The particle positions are chosen initially to correspond to a Bennett distribution. As the beam propagates, the particles may evolve into any configuration consistent with axisymmetry. Scattering of beam electrons

by air molecules can be included in the code, but for most of the cases run this feature is turned off in order to simplify the analysis. The result of scattering is Nordsieck expansion of the beam.[16-18] Usually this occurs slowly compared to instability growth, but we do discuss some cases in which the onset of the hollowing instability is delayed, and slow increase of the beam radius can influence the instability. Because scattering in the simulation is the cumulative effect of a large number of small angle scattering events over the length of a time step, we have treated the effect by use of a probability function $P[\delta(\gamma\vec{v})]$ giving the probability that the change of the momentum of a beam particle during a time step is $\delta(\gamma\underset{\sim}{v}_\perp)$. We specify that

$$P(\delta(\gamma\vec{v})) = \alpha \exp\{-\beta^2[\delta(\gamma\vec{v}_\perp)^2]\}.$$

The distribution width is related to the increase in perpendicular energy of a beam particle by scattering, δE, by the equation

$$\delta E = \langle\delta(\tfrac{1}{2}\gamma m_e \vec{v}_\perp^2)\rangle = \frac{m_e}{2\gamma}\langle\delta(\gamma\vec{v}_\perp)^2\rangle$$

The quantity, δE, has been evaluated[15,16] as

$$\delta E = \frac{e^2}{\gamma m_e^2}\frac{2C_N}{\lambda_r}\delta t$$

where $C_N = 3.7 \times 10^{19}$ ergs/sec is the Nordsieck constant, δt is the time interval over which the scattering takes place, and λ_r is the radiation length, given by

$$\lambda_r = \left[4nZ(Z + 1) \left(e^2/ c\right)(e^2/m_e c^2) \ln \left(\frac{137}{Z}\right)^{1/3}\right]^{-1}$$

where n is the gas density and Z is the effective charge number of the gas.

3. General Features of the Instability in Uniform Gas

Figure 1 shows a global picture of the instability evolution for a typical unstable case, a beam with I_b = 20 kA, Bennett radius a = 0.5 cm (in the well-pinched part of the beam), rise time $\tau_r = 0.25 \times 10^{-9}$ sec, and electron energy E = 50 MeV propagating in uniform cold air at density 760 torr. The figure is a surface plot of $r_{1/2}(\zeta,z)$, the median radius of the beam slice at position ζ behind the beam head, at propagation distance z. Note that only the first 45 cm, i.e. 1.5 nsec, of the beam is shown, since the instability grows so rapidly in ζ. The beam is injected with Bennett radius and perpendicular temperature independent of ζ, i.e. uniform emittance. At ζ = 45 cm, the beam is fairly well matched to the net current and close to Bennett equilibrium; initially it expands and oscillates at amplitude ~ 10% about the equilibrium value of $r_{1/2}$, due to a slight initial overpressure. Near the pinch point ($\zeta \approx 8$ to 12 cm), however, there is considerably more plasma return current, the net current is thus smaller and the beam is significantly overpressured. It thus expands and oscillates at an initial amplitude of ~ 50%. The instability grows out of these oscillations. It is initiated a few centimeters behind the pinch point, and the waves grow as they propagate backward in the beam, rapidly reaching very large amplitude. This behavior is evident in Fig. 1, but is perhaps seen more clearly in Fig. 2, where $r_{1/2}$ is shown as a function of z for four different beam slices at ζ = 8, 15, 25, and 40 cm.

The initiation of the instability at moderately large amplitude is probably typical of experimental conditions, since it is difficult to impossible to produce a uniformly well-matched beam. However the magnitude of the initial mismatch does not appear to play any role in determining whether a beam will go unstable. In other cases, we have taken care to match the

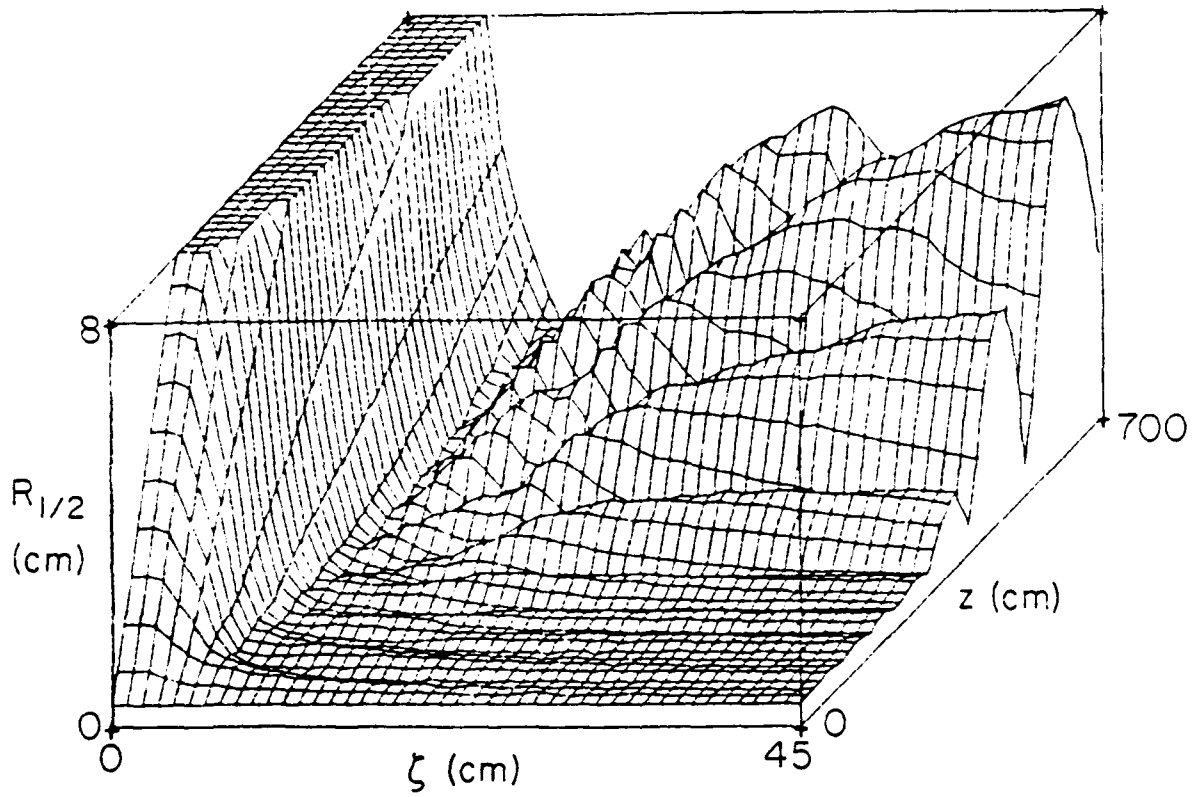

Fig. 1 — Surface plot of beam median radius $r_{1\,2}$ as a function of z and ζ, for a beam with I_b = 20 kA, a = 0.5 cm, rise time 0.25 nsec, propagating in air at ambient density. The beam energy is 50 MeV. Scattering of beam electrons is not included.

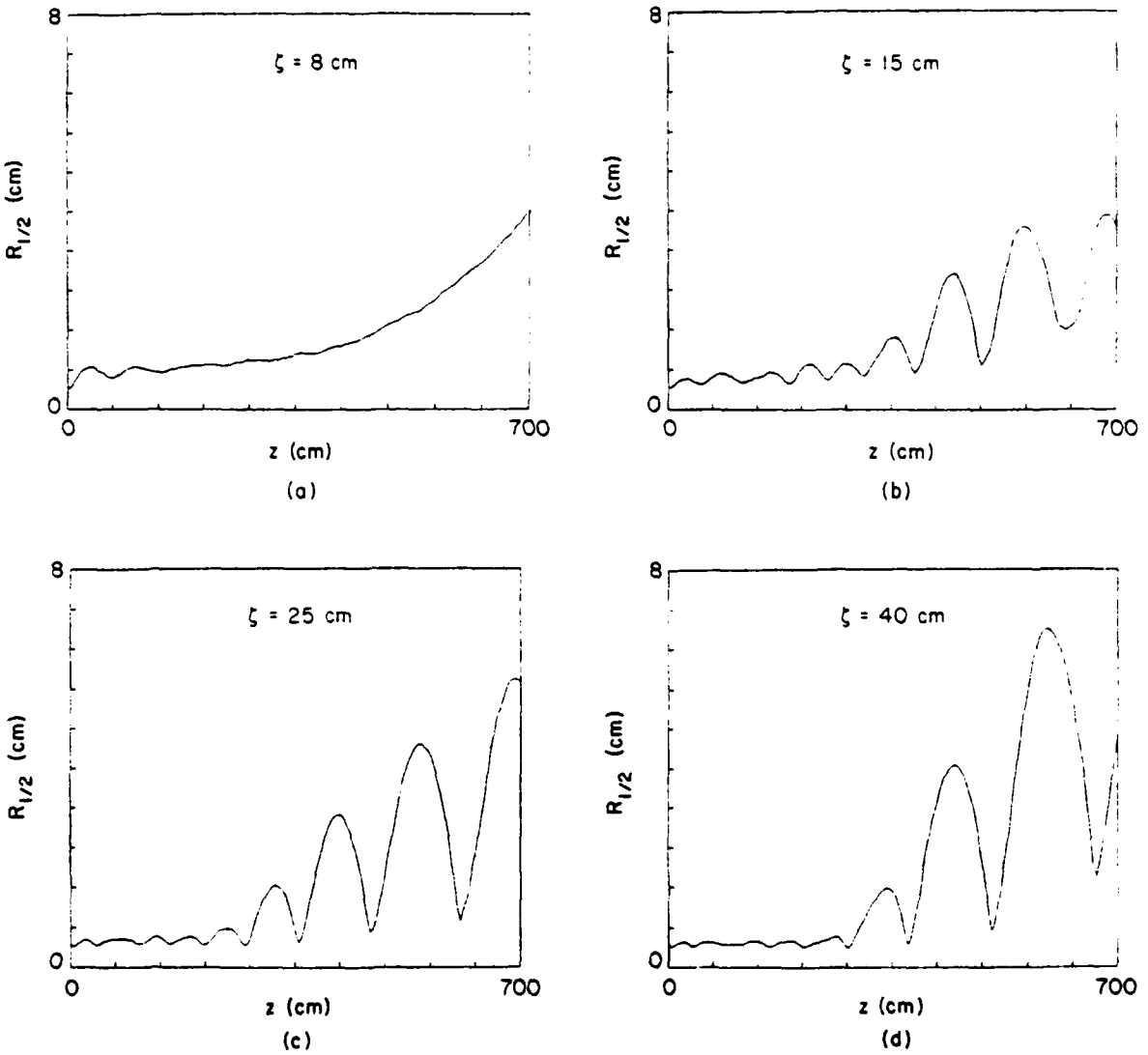

Fig. 2 — Plots of beam radius $r_{1/2}$ as a function of z for various values of ζ, for the same case as Fig. 1

initial conditions carefully so that the initial radial oscillations near the pinch point are small. We then find that it takes a good deal longer (in z) before the instability grows out of the noise, but that once it does the subsequent evolution is quite similar to that seen in Figs. 1 and 2. In no case have we found an unstable set of beam and gas parameters to be stabilized (or vice-versa) by changing the amplitude of the initial oscillations. We thus infer that the observed wave growth is indicative of a linear instability, although it is important to note that the phenomena that are clearly visible in these simulation studies are associated with large-amplitude nonlinear evolution of the instability; behavior in the small-amplitude regime is largely obscured by noise, unless special techniques[9] are used to make it visible.

We note that the unstable region is behind the pinch point, so that $4\pi\sigma a/c \gg 1$ throughout most of the region, and electrostatic neutrality prevails. We also note, to be elaborated later, that avalanche is important near the pinch point, but that instability growth occurs mainly in a region where E_z is relatively small and further conductivity generation is dominated by direct ionization (except for cases at density $\lesssim$ 50 torr). Thus the main premises of the calculation of our companion paper[8] are satisfied. However that calculation predicts that the sausage mode (m = 0, n = 1) is stable in the region of observed instability in the simulations with density $p \geq 50$ torr. This is our first indication that another mode is responsible for the instability.

It is of interest to compare the evolution of the instability within each beam slice as a function of propagation distance z (which can be thought of as playing the role of time in beam dynamics), $r_{1/2}(z)$ for various choices of ζ shown in Fig. 2, with the "snapshots" of the beam $r_{1/2}(\zeta)$ for various

choices of z shown in Fig. 3. We note first the behavior at $\zeta = 8$ cm, just in front of the unstable region, shown in Fig. 2a. Here the initial radial oscillations decay, as would be expected due to phase mixing. (Here $\zeta = 8$ lies just at the initial pinch point, and $r_{1/2}$ slowly increases as erosion proceeds.[1,19] Further back in ζ the oscillations of $r_{1/2}(z)$ go unstable, but they remain coherent and roughly sinusoidal. At any given time the oscillation frequency Ω is roughly equal to the betatron frequency at that time. All of this is indicative of a narrow Ω-spectrum of unstable oscillations, in agreement with the predictions of linear theory for all return-current-driven instabilities.[12] Since the oscillation amplitude is large, however, a number of nonlinear modifications occur. The betatron frequency is inversely proportional to $r_{1/2}$, which causes the wave period to increase as the amplitude increases, and the wave form to be flattened at the crests and sharpened at the troughs. The waves grow rapidly to catastrophic amplitude (typically ~ 10 oscillations), but wave growth is not exponential, as would be expected in the small-amplitude regime. In contrast to the behavior seen in Fig. 2, the plots of $r_{1/2}(\zeta)$ in Fig. 3 show a disturbance propagating back in ζ, but with an irregular structure in ζ that does not single out any particular mode as dominant. This is again characteristic of linear theories of the return-current-driven instabilities[12], which predict a broad spectrum of unstable wavelengths in ζ, ranging from about the local value of $\pi\sigma\, r_{1/2}^2/c$ to infinity. Any disturbance in this range that happens to be initiated will grow.

There are other ranges of beam and gas parameters for which the instability does not occur. The distinction between stable and unstable cases is very clear in an $r_{1/2}(\zeta,z)$ surface plot. Figure 4 shows a typical stable case. It differs from the case of Fig. 1 only in that the beam current is 10

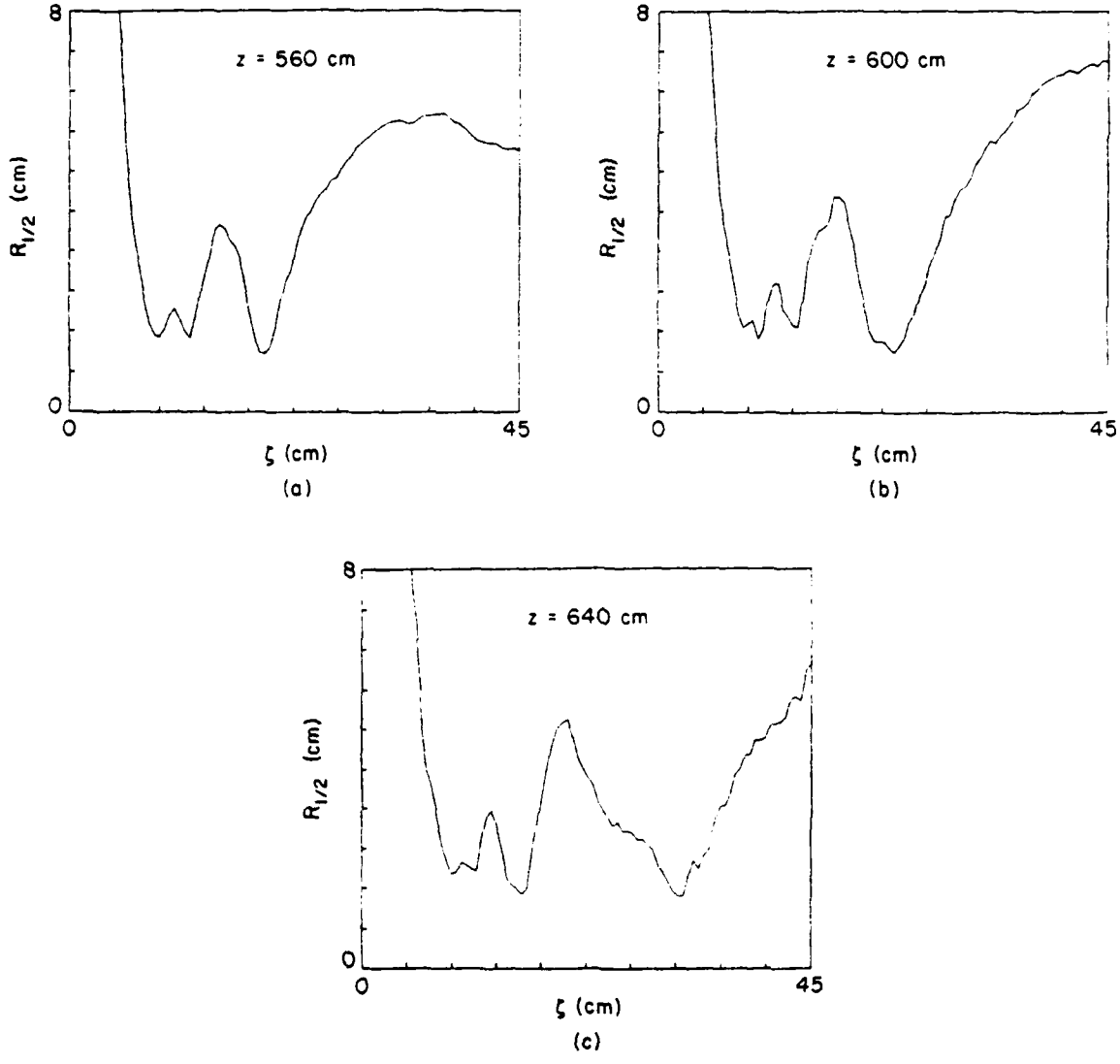

Fig. 3 — Plots of beam radius $r_{1/2}$ as a function of ζ for various values of z, for the same case as Fig. 1

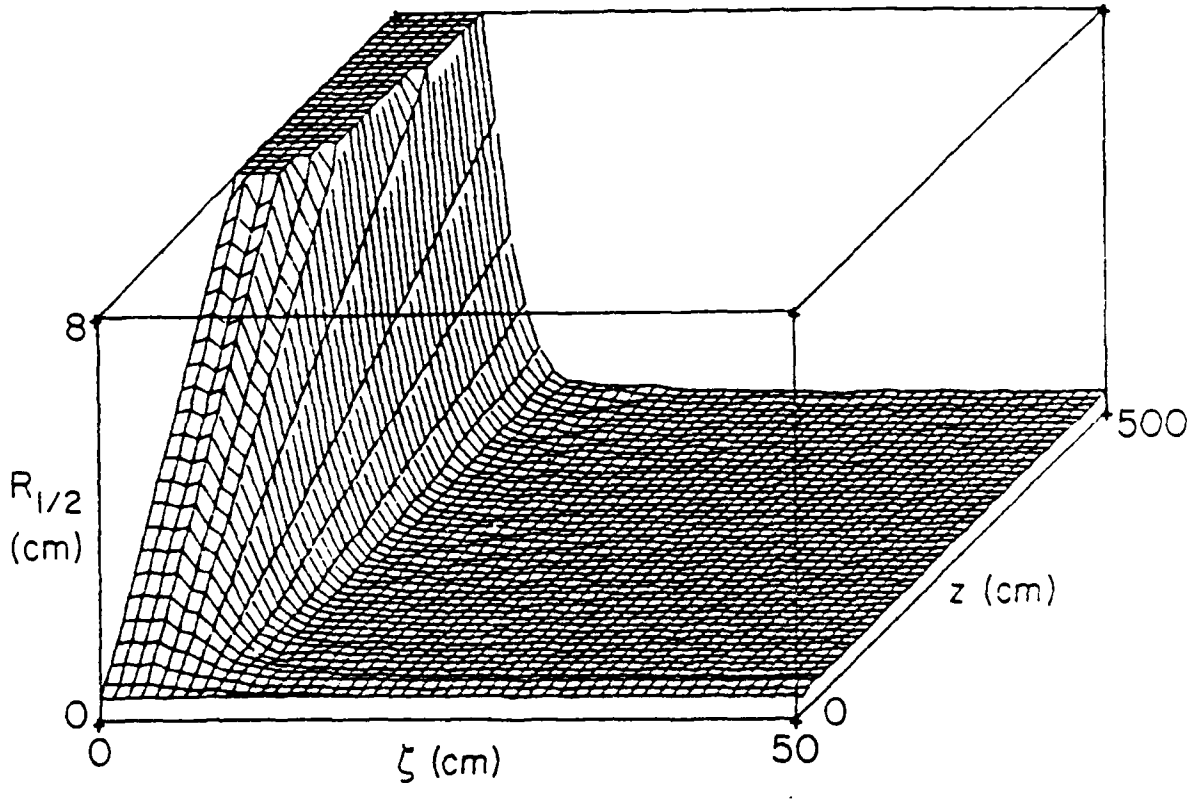

Fig. 4 — Surface plot of $r_{1/2}(\zeta,z)$ for the stable case I_b = 10 kA, a = 0.5 cm, rise time 0.25 nsec, propagating in ambient density air

kA, rather than 20 kA as in Fig. 1. We see that the initial oscillations simply decay away, due to phase mixing. At the borderline between stable and unstable parameters, we find marginally stable cases where fluctuations persist for a long time, but without any real growth. Later we shall give a survey of stable and unstable cases and discuss the determining factors as to stability.

Figure 5 shows surface plots of beam current density $J_b(r,\zeta)$ at five successive values of z, for the case of Fig. 1. This diagnostic provides a more detailed picture of the instability. We see that the unstable oscillations are not at all like the sausage mode, i.e. like self-similar radial oscillations of the beam. On the contrary, the instability begins in a region where the net current in the central (near-axis) region has a downward fluctuation, causing the pinch force to weaken and the beam to hollow out as we move back in ζ. At each subsequent oscillation, the beam profile alternately assumes a hollowed annular shape and then a tightly compressed shape strongly peaked on axis.

These observations strongly suggest that the observed unstable wave growth results from a linear instability of the hollowing mode. However they do not absolutely exclude the $m = 0$, $n = 1$ sausage mode as a source of instability, since various modes can be coupled in the large-amplitude regime, and thus the observed large-amplitude hollowing mode could conceivably grow out of an initial sausage instability. To determine whether there is any involvement of the sausage mode, we have performed the following additional simulation test. We modify SIMMO by calculating $J_b(r,\zeta,z)$ from a beam envelope of Bennett shape which expands and contracts self-similarly in accordance with the envelope equations of Lee and Cooper[16] rather than from a collection of simulation particles. This permits the beam to oscillate in

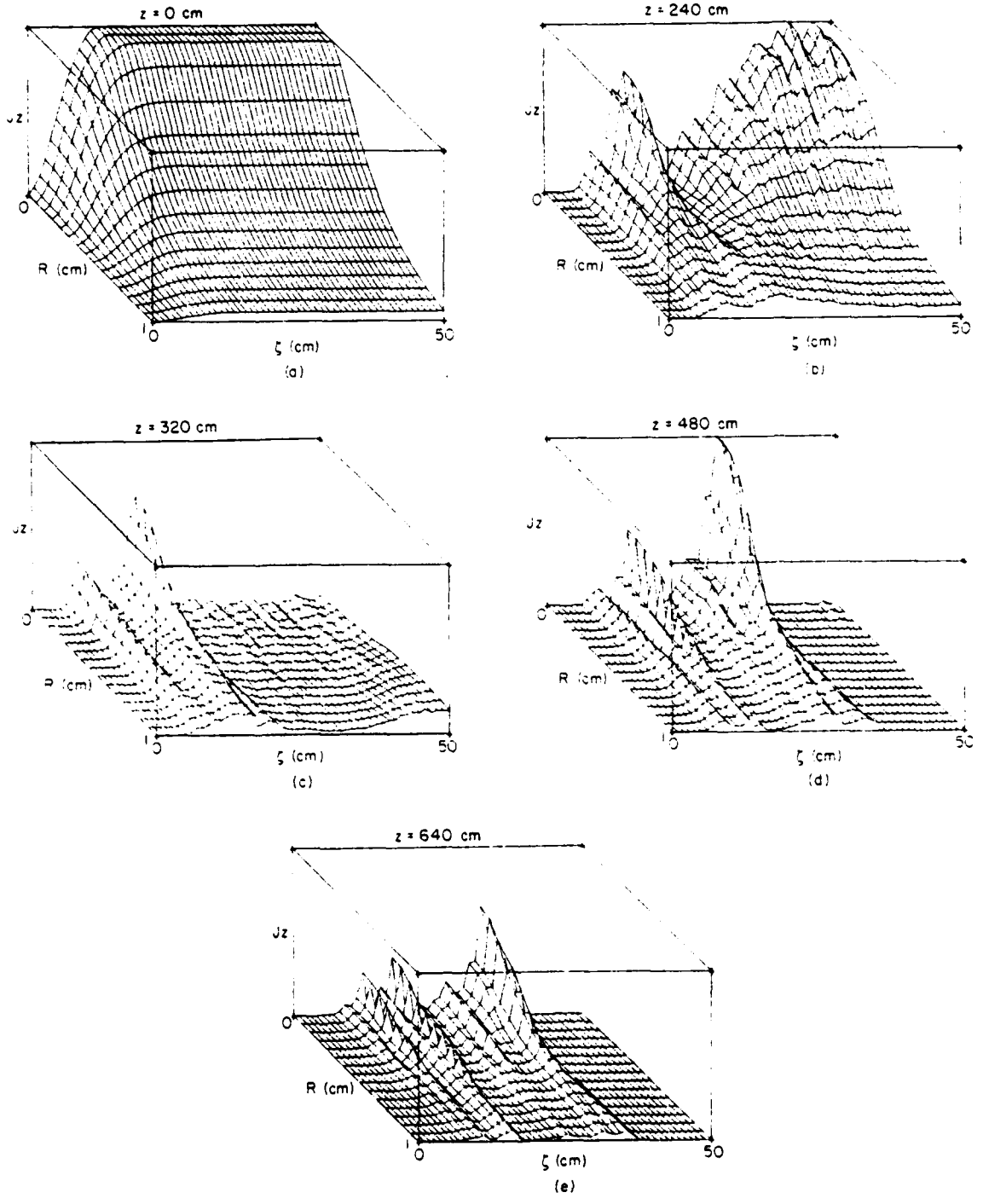

Fig. 5 — Beam current density contours J_b (r,ζ) for various values of z, for the same case as Fig. 1

reasonably close approximation to the sausage mode, but not to distort as required by the higher m = 0 modes. We then find that all cases studied are stable, with $r_{1/2}(\zeta,z)$ plots similar to Fig. 4. We conclude that the sausage mode is indeed stable, and that the instability observed is entirely due to the hollowing mode. This conclusion is entirely consistent with our calculation of Ref. 8, which indicates that the sausage mode should be stable for this case. Unfortunately no fully adequate linear theory of the hollowing mode is available at present. Thus we shall rely on simulations to elaborate on the properties of the instability.

4. Importance of Avalanche as the Destabilizing Mechanism

Table 1 summarizes the results of a large number of simulations with I_b varying from 10 kA to 100 kA and air density ρ varying from 760 torr to 10 torr. In all cases here the beam radius a = 0.5 cm, the rise time of I_b is 0.25 nsec, the beam energy is 50 MeV, and the beam propagates in uniform neutral air. We note that a 10 kA beam with these characteristics is unstable only for air in the density range 500 torr $\gtrsim \rho \gtrsim$ 75 torr. The upper limit of the unstable range would appear at first sight to be simply a requirement that the return current fraction be large. We define an effective pinch current I_{eff} in terms of the J_b-weighted pinch force,

$$I_{eff} = \int_o^\infty dr 2\pi r \, [J_b(r)/I_b] \int_o^r dr' 2\pi r' \, [J_b(r') + J_p(r')]. \qquad (20)$$

If $J_b(r)$ and $J_p(r)$ have identical profiles, I_{eff} reduces to $I_{net} \equiv I_b - I_p$, but in practice the equilibrium profiles of J_b and J_p are very similar out to one or two Bennett radii, while at large r, $J_p(r)$ has a low-amplitude tail that can carry a good deal of current while exerting little force on the beam; hence the importance of distinguishing between I_{net} and I_{eff}. Usually $J_{net}(0)/J_b(0)$ is a very good approximation to I_{eff}/I_b though. We shall also find it useful to define an effective plasma current $I_{pe} \equiv I_b - I_{eff}$. Uhm and Lampe[12] have shown that even in the worst case where $\sigma(r)$ is taken to be independent of ζ and z, and $J_b(r)$ has a flat-topped profile, the hollowing mode is unstable only if

$$I_{eff}/I_b \leq 0.62. \qquad (21)$$

When the stabilizing effects of self-consistent conductivity evolution and

(U) Table 1

Summary of simulation results for beams with well-pinched radius a ≈ 0.5 cm and I_b rise time 0.25 nsec. In the last column, U and S indicate unstable and stable cases, respectively.

I_b(kA)	ρ (torr)	I_{eff}/I_b	E_z/ρ	Stability
100	760	.09		U
40	760	.18	.12 - .15	U
20	760	.35	.10 - .14	U
10	760	.5	.10 - .11	S
10	600	.49	.10 - .13	S
10	500	.48	.11 - .17	U
10	400	.40	.12 - .23	U
10	200	.27	.17 - .31	U
10	100	.22	.38 - .48	U
10	75	.21	.48 - .49	U
10	50	.20	.50 - .97	S
10	10	.08	3.8 - 9.0	S

rounded beam profiles are considered, one might expect to find a somewhat more stringent instability condition. Indeed our simulation results, as reported in Tables 1-3 and in other cases, do indicate that

$$I_{eff}/I_b \lesssim 0.50 \qquad (22)$$

is a necessary condition for instability, and the requirement Eq. (22) would appear to define a maximum air density for instability. However the situation is really not that simple. The 10 kA beam of Table 1 is stable at 50 torr and even at 10 torr, where I_{eff}/I_b is very small, so Eq. (22) is clearly not a sufficient condition for instability. This is quite a surprise, and cannot be explained by any of the preceding literature. A second surprise was found when we repeated some of the simulation runs with avalanche turned off, i.e. the second term of the conductivity equation (14) deleted. We then find all cases to be stable, even those with I_{eff}/I_b very small, e.g. for I_b = 100 kA, ρ = 760 torr as reported in Table 2. Thus the presence of avalanche is essential to the instability.

To elucidate this puzzling dependence on avalanche, we have done some further numerical experiments. Avalanche often dominates $d\sigma/d\zeta$ near the pinch point, where $E_z(\zeta)$ has a sharp spike[1,19], but typically is negligible further back in the beam where most of the instability growth takes place, for air densities $\gtrsim$ 50 torr. This is illustrated in Fig. 6, where $\sigma(r = 0, \zeta, z = 0)$ is plotted for the 100 kA case of Table 2 with and without avalanche. To determine whether the small continuing contribution of avalanche to $\partial\sigma/\partial\zeta$ in the region $\zeta > 20$ cm (where most of the instability growth occurs) plays an important role, we ran a 40 kA case (see Table 2) in which we replaced the second term of Eq. (14) with

$$(\partial\sigma/\partial\zeta)_{\text{avalanche}} = \nu_i \sigma [1 - \exp(-\zeta^2/100)], \qquad (23)$$

i.e. we allowed the normal avalanche process to proceed for $\zeta \lesssim 10$ cm but turned avalanche off rather sharply for larger values of ζ. This case was found to be unstable, and in fact qualitatively indistinguishable from the case with full avalanche. We thus conclude that avalanche is an essential factor for instability, but only because it leads to a destabilizing initial condition on $\sigma(r, \zeta)$ that somehow preconditions further growth in ζ.

The obvious way in which avalanche could lead to instability is by causing a rapid conductivity rise in the beam head, leading to increased I_{pe}/I_b, but this does not seem very convincing since we have shown that even cases with very large I_{pe}/I_b can be stable. To probe the mechanism further, we tried another numerical experiment to determine whether modification of the radial conductivity profile by avalanche is the crucial effect. Indeed avalanche is normally strongest on axis, because the electric field $E_z(r)$ typically varies as[1,19]

$$E_z \propto \ln\left[\frac{1 + b^2/a^2}{1 + r^2/a^2}\right] \qquad (24)$$

and thus has a gentle peak at $r = 0$. [In (24), b is the outer radius of the conductivity channel, where $4\pi\sigma r/c = 1$; generally, $b/a \gg 1$.] This weak variation of $E_z(r)$ has usually been ignored in theoretical models but could lead to non-negligible radial variation of the avalanche coefficient ν_i, which from Eqs. (16) - (17), is a very sensitive increasing function of E/p. The peaking of ν_i on axis would then tend to narrow the radial profile of conductivity. To test this hypothesis, we replaced $\nu_i(r, \zeta, z)$ in Eq. (14) by $\nu_i(0, \zeta, z)$, thereby eliminating the on-axis peak of ν_i, but increasing the

(U) Table 2

Summary of simulation results. Either avalanche is included as specified in Eqs. (14), (16) and (17), denoted "yes"; or avalanche is completely omitted, denoted "no"; or avalanche is turned off according to Eq. (23) for $\zeta >> 10$ cm, denoted "partial".

I_b(kA)	P(torr)	a	Avalanche included?	I_{eff}/I_b	Stability
20	760	0.5	yes	0.35	U
20	760	0.5	no	0.40	S
100	760	0.5	yes	0.09	U
100	760	0.5	no	0.13	S
40	760	0.5	yes	0.18	U
40	760	0.5	partial	0.20	U
40	760	0.5	no	0.24	S

(U) Table 3

Summary of simulation results where the well-pinched beam radius a is varied. In the last column stable, marginally stable, and unstable cases are denoted by S, S(M), and U, respectively.

I_b(kA)	ρ(torr)	a(cm)	I_{eff}/I_b	$E_z/\rho(\frac{MV/cm}{atm})$	Stability
10	200	0.5	.27	.16 - .33	U
10	200	1.0	.40	.09 - .21	U
10	200	1.5	.46	.07 - .15	S(M)
10	200	2.0	.48	.05 - .11	S
10	760	0.2	.35	.11 - .15	U
10	760	0.5	.50	.10 - .11	S
20	760	0.5	.35	.10 - .14	U
20	760	1.5	.39	.03 - .06	S

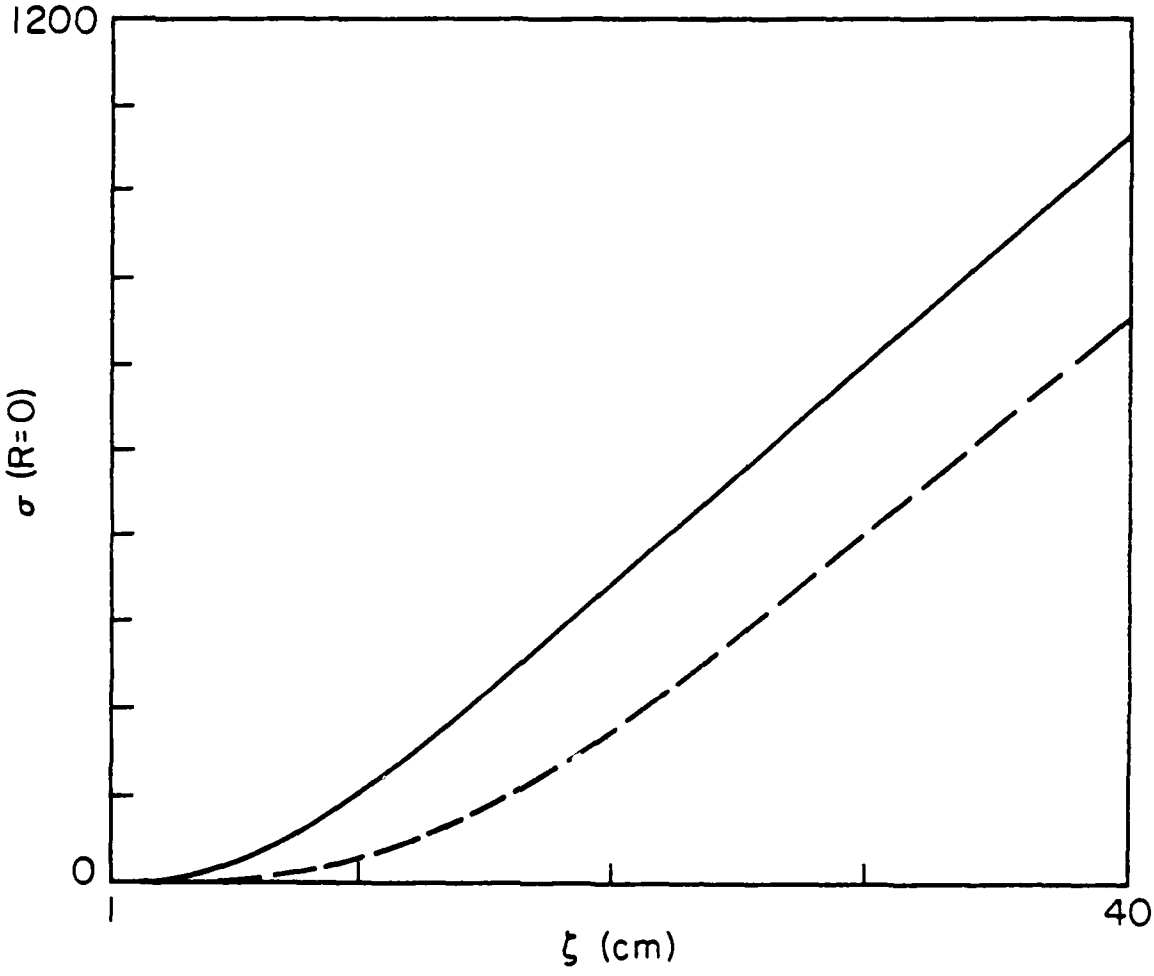

Fig. 6 — Conductivity $\sigma(r=0)$ as a function of ζ, with avalanche included (solid curve) or omitted (dashed curve), for a 100 kA beam with pinched radius a = 0.5 cm propagating in ambient density air

overall amount of avalanche. All cases studied then became stable. We conclude that the hollowing instability is indeed triggered by conductivity profile narrowing due to the on-axis peak of avalanche ionization. One can well understand that conductivity narrowing would lead to narrowing of the profile of $J_p(r)$ compared to $J_b(r)$, and thus weaken the pinch force in the central core of the beam, thereby exciting a hollowing of the beam.

This analysis can also explain the absence of instability in the 10 torr case of Table 1. Here E/ρ is very strong, and avalanche is very rapid, but according to Eqs. (16)-(17) the sensitivity of the avalanche rate ν_i to E/ρ, that is $d\ \ln\ \nu_i / d\ \ln\ (E/\rho)$, becomes relatively weak. Apparently the resulting on-axis conductivity peaking is insufficient to excite the instability for E/ρ above some critical value.

Given the insight that instability occurs if the peak value of E/ρ in the E_z spike is large enough to excite strong avalanche, but not so large as to weaken the radial peaking of ν_i, we have searched the "data base" provided by the simulations of Tables 1 and 3 for an empirical instability criterion. We find necessary and sufficient criteria for instability to be that Eq. (22) is satisfied and that at the same time

$$130\ \text{kV/cm-atm} \lesssim E/\rho \lesssim 500\ \text{kV/cm-atm} \qquad (25)$$

at the E_z spike. Usually (but not always) Eq. (22) is satisfied if Eq. (25) is satisfied. As will be seen later, these criteria summarize the instability threshold as a function of I_b, ρ, a, rise time, and beam energy E. In order to determine whether the instability criteria are satisfied, it is not necessary to run a particle simulation code; a fast running axisymmetric envelope code will suffice, although such a code will never actually show

instability growth. The reader is cautioned, however, that the initial values at $z = 0$ of E/ρ and I_{eff}/I_b can be misleading. Typically E/ρ increases and I_{eff}/I_b decreases as erosion proceeds, so that an initially stable beam can go unstable as z increases.

5. Dependence of the Instability on Beam Parameters

We have seen that increasing the beam current tends to lead to instability. Other parameters which may affect the stability properties are the equilibrium beam radius, the rise time of the current, and the beam energy.

The peak magnitude of the electric field near the pinch point decreases if the beam radius is increased and other beam parameters are held fixed. The consequent reduction in avalanche strength also tends to decrease the plasma current and thus raise I_{eff}/I_b, particularly for beams with $I_b \lesssim 10$ kA is reduced-density air. (The effect is much weaker for higher-current beams in full-density air.) This suggests that the unstable range seen in Table 1, 500 torr $\gtrsim \rho \gtrsim$ 75 torr for a = 0.5 cm, can be shifted to lower pressures by increasing the beam radius. This suggestion has been verified, as is seen in Table 3, which shows some cases identical to those of Table 1 except for the beam radius a. We note, for example , that a beam with I_b = 10 kA, ρ = 200 torr is marginally stable with a = 1.5 cm and is distinctly stable with a = 2.0 cm. In this case both instability conditions Eqs. (22) and (25) fail when a = 2.0 cm. For I_b = 20 kA at ρ = 760 torr, a beam with a = 1.5 cm is stable; even though condition Eq. (20) is satisfied, the avalanche condition Eq. (23) is not.

Except for beams with extremely short rise time (< 0.2 nsec), the pinch point initially falls in a region near the beam head where I_b is well below its peak value. The height of the E_z spike and (to a lesser degree) the value of I_{eff} are determined by the value of I_b <u>at the pinch point</u>, not by the nominal beam current. Thus beams with slower rise time are often found to be stable in their initial state because E/ρ is too small to satisfy Eq. (23), even though a very fast-rising beam with otherwise the same parameters (Tables

1-3) is unstable. The beam radius may change during propagation because of Nordsieck expansion due to the collisions of beam particles with the background gas.[16-18] If the effect of Nordsieck expansion is negligible on the time scale of interest, the height of the E_z spike typically increases appreciably as the pinch point erodes back in the beam and thus moves into a region of larger I_b. As a result, a beam which is initially stable can go unstable at a later time when E/ρ becomes large enough to satisfy Eq. (23). On the other hand, if Nordsieck expansion causes the radius to increase appreciably on the same time scale on which I_b is increasing at the pinch point, the E_z spike may never become large enough to satisfy Eq. (23).

Figure 7 shows the median radius $r_{1/2}(\zeta,z)$ for a beam with I_b = 10 kA, energy 50 MeV, rise time 0.25 nsec and pinched radius 0.5 cm propagating in 500 Torr air with scattering turned on. The pinched radius increases with propagating distance, and the beam is stable due to the effect of Nordsieck expansion. A comparison with Table 1 shows that a beam with these parameters is unstable if scattering is not included.

To our knowledge, the instability depends on the beam energy only through the effect that nose erosion and Nordsieck expansion have on delay onset. For cases in which the instability occurs promptly, the beam energy appears to have no effect on the instability threshold.

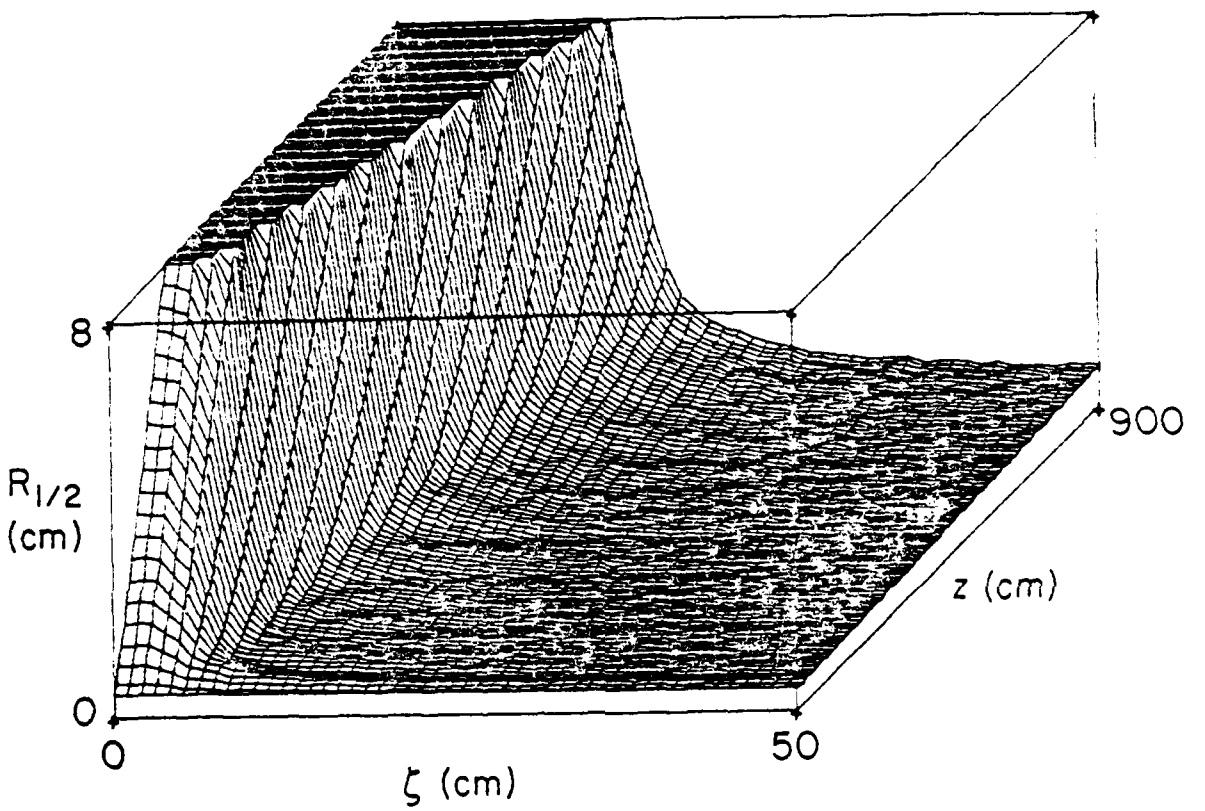

Fig. 7 — Plot of beam median radius $r_{1/2}$ (ζ,z) for a beam with I_b = 10 kA. energy 50 MeV. rise time 0.25 nsec and initial pinched radius 0.5 cm, propagating in 500 torr air. Note the increase of $r_{1/2}$ with z, due to Nordsieck expansion, which is responsible for the stability of this case.

6. Delta-Ray Contributions to Conductivity

The conductivity physics embodied in Eqs. (14)-(17) is very crude, and was chosen primarily for simplicity and to facilitate comparison with code work at other laboratories. Two obvious improvements would be to use a temperature-dependent formulation[14] for σ, and to use a more accurate formulation of the avalanche ionization which has recently become available.[14] We plan to re-examine these points in future work. It appears that they result only in fairly small numerical changes in the instability thresholds, and not in fundamental changes.

On the other hand, it would appear that significant stabilizing effects might result from the inclusion of delta-ray contributions to the plasma conductivity. Delta-rays (i.e. high-energy secondary electrons) can in some situations (particularly at reduced density), spread out the deposition of beam energy so as to broaden the profile of plasma conductivity, delay the process of energy deposition, and carry significant current themselves. Modeling of these phenomena has been a subject of recent interest, but quantitative results are, for the most part, not available yet. We have therefore chosen to test the first of these effects (conductivity spreading) by introducing a simple parametrized model, and varying the parameter to simulate various degrees of nonlocal beam energy deposition. To this end, we replace Eq. (14) by

$$\frac{\partial}{\partial \zeta}\,\sigma(r,\zeta,z) = \kappa \int_0^\infty dr' 2\pi r' J_b(r',\zeta)(\pi R_\delta^2)^{-1} \exp\left[-(r-r')^2/R_\delta^2\right]$$

$$+ \nu_i(r,\zeta,z)\,\sigma(r,\zeta,z); \qquad (26)$$

R_δ is then some assumed average delta-ray mean free path.

We find that for a typical unstable case, I_b = 20 kA, ρ = 760 torr, a = 0.5 cm, the beam can be stabilized in this way, but only for $R_\delta \gtrsim 2a$. For smaller values of R_δ, the delta-ray spreading effect is simply overwhelmed by the effect of avalanche. This is rather more delta-ray spreading than would be expected, except possibly for small radius beams in low density gas, so this does not appear to be an important stabilizing mechanism - although a final decision should await numerical evaluation of delta-ray effects in various parameter regimes.

7. Stabilization by Emittance Tapering

According to the analysis of Sec. 4, the hollowing instability is triggered by a slight narrowing of the conductivity profile, as compared to the beam profile, in the crucial region behind the pinch point. If the beam parameters could be altered in such a way as to broaden the $\sigma(r)$ profile there, the instability could be avoided. Since $\sigma(r)$ at a given ζ depends on the beam profile at earlier ζ-points, one way to do this is to prepare a beam whose emittance decreases with increasing ζ, so that the beam radius tapers down from the head of the beam. We have tested this hypothesis by running a simulation with I_b = 10 kA, ρ = 100 torr, and equilibrium beam radius given by

$$a(\zeta) = (0.5\ \text{cm})\ \{1 + 3\ \exp\ [-\ \zeta^2/(7.5\ \text{cm})^2\ ]\}. \qquad (27)$$

This beam was found to be stable, even though a beam with uniform emittance and with the same radius at the pinch point (1.0 cm) would be unstable, and even though both instability criteria Eqs. (22) and (25) were satisfied.

3. Status of Experiments

The principal experimental data available at present are from the FX-25 diode beam experiments[20] at Livermore several years ago. The beam's nominal parameters were I_b = 10-15 kA, electron energy 1.5-2 MeV, pulse width ~ 30 nsec, risetime 5 nsec (but steepening to $\lesssim$ 1 nsec after propagating under some conditions). The propagation experiments concentrated heavily on the low-density regime 1-20 torr, although densities up to 500 torr were examined. Increasingly strong hose instability was observed as the density was increased above 10 torr. At densities well above 20 torr, the beam was essentially lost after propagating less than 0.5 m; this was attributed to hose. At still higher densities, our analysis would predict hollowing instability for the very fast-rise-time cases. There are no reported observations of the hollowing mode, but it should be noted that at the time of the experiment the axisymmetric modes had not been analyzed and interest was focused on the hose instability. Perhaps more to the point, in an unconditioned diode beam such as the FX-25 hose can be initially excited at large amplitude and would thus destroy the beam rapidly enough to obscure the hollowing mode, which could also have been present. Experiments in this regime with a well-conditioned fast-rising beam from the ETA accelerator[21], which should be available in the near future, are more likely to be dominated by hollowing instability rather than hose.

The theoretical situation at air density $\lesssim$ 10 torr is a bit uncertain at present. Our initial simulations with short segments ($\lesssim$ 2 nsec) of fast-rising beam pulses, e.g. the 10 torr case of Table 1, showed striking stability, in agreement with the experimental conclusions available. However in recent work we have been exploring a wider range of parameters and longer beam segments in an attempt to define appropriate low-density experiments that

could be performed at the present time. We have found several cases where axisymmetric instability develops in the simulations, but the instability is typically slower-growing and may not be the same type of hollowing instability discussed in this paper. Also, plasma currents that are not described by the simple conductivity model of Eqs. (14) - (17) may play a role in this regime, as mentioned in Sec. 6. It is our intention to defer detailed discussion of axisymmetric instability in this low density regime, and implications for past and present experiments, to a separate report.

9. Conclusions

We have demonstrated that under certain conditions a beam propagating in air is subject to a strong axisymmetric hollowing instability. When the instability is present, it grows a few centimeters behind the pinch point and effectively destroys the entire beam within a few meters of propagation. The instability occurs when there is strong avalanche which peaks on axis and thus causes the plasma return current to flow with a narrower profile than the beam; this leads to the condition that E/p be in the range 130 to 500 kV/cm-atm at the E_z spike at the pinch point, Eq. (25). It is also necessary that there be a strong plasma current ($I_{eff}/I_b \lesssim 0.50$), Eq. (21), but this is usually guaranteed by the presence of strong avalanche. These two conditions delineate, for a beam of uniform emittance propagating in uniform air described by the simple conductivity model of Eqs. (14) - (17), a regime of instability that depends on the three parameters I_b (at the pinch point), p and a. The unstable density range runs from 75 to 500 torr for a fast-rising 10 kA, $a = 0.5$ cm beam, and shifts downward for beams with larger radius, as seen in Table 3. If the instability conditions are not satisfied initially because I_b at the pinch point is too small (for cases of long rise time), they may be satisfied at a later time when the pinch point erodes[1,19] back to a region of higher I_b; however Nordsieck expansion[17] can frustrate this process by simultaneously increasing a. To determine whether a particular set of parameters satisfies the two instability conditions it is not necessary to run a full axisymmetric simulation; an axisymmetric envelope code will do.

We expect some weak dependence of the stability limits on the values of the direct and avalanche ionization coefficients and the electron mobility used in the conductivity model Eqs. (14) - (17). This has not yet been explored in detail. We have shown that radial conductivity spreading due to

delta rays could in principle stabilize the instability if the effect were strong enough, but that the amount of spreading expected does not appear to have a strong effect.

Although these simulations have elucidated the physics of the hollowing instability, a linearized normal mode theory would significantly increase our understanding. We are working to develop such a theory at present.

A variety of additional studies are in progress, including the effects of plasma current modifications due to recombination, temperature-dependent collision cross-sections, and nonlocal electron transport, and more detailed and extensive simulation modeling of actual experimental pulse shapes and dependence on rise time.

Acknowledgments

We are pleased to acknowledge many helpful discussions and comparisons of simulation code results with Dr. Frank W. Chambers, as well as much interaction with Drs. Richard F. Hubbard and William M. Sharp. We are also grateful to Prof. Keith M. Brueckner for sharing his simulation results with us.

References

* Supported by Defense Advanced Research Projects Agency under ARPA order 4395, Amendment No. 1.

1. W. M. Sharp and M. Lampe, Phys. Fluids Fluids 23, 2383 (1980).
2. E. S. Weibel, Phys. Rev. Lett. 2, 83 (1959)
3. G. Benford, Plasma Phys. 15, 483 (1973).
4. R. Lee and M. Lampe, Phys. Rev. Lett. 31, 1390 (1973).
5. R. F. Hubbard and D. A. Tidman, Phys. Rev. Lett. 41, 866 (1978).
6. E. P. Lee, S. Yu, H. L. Buchanon, F. W. Chambers and N. M. Rosenbluth, Phys. Fluids 23, 2095 (1980).
7. K. A. Brueckner, N. Metzler and R. Janda, Phys. Fluids 24, 964 (1981).
8. M. Lampe and G. Joyce, Phys. Fluids, this issue.
9. F. W. Chambers, "Sausage Mode Stability Boundaries: Enumeration and Verification", Lawrence Livermore National Laboratory Report UCID-18879 (1980).
10. K. A. Brueckner, private communication.
11. G. Joyce, M. Lampe, W. Sharp and H. S. Uhm, Bull. Am. Phys. Soc. 26, 915 (1981).
12. H. S. Uhm and M. Lampe, Phys. Fluids 25, 1444 (1982).
13. E. P. Lee, "The New Field Equations", Lawrence Livermore National Laboratory Report UCID-17286 (1976).
14. A. W. Ali, "Electron Avalanche Ionization of Air and a Simple Air Chemistry Model", Naval Research Laboratory Memorandum Report 4794 (1982).
15. F. W. Chambers, "Mathematical Models for the RINGBEARER Code", Lawrence Livermore National Laboratory Report UCID-18302 (1979).
16. E. P. Lee and R. R. Cooper, Particle Accelerators 7, 83 (1976).
17. E. P. Lee, Phys. Fluids 19, 60 (1976).

18. M. I. Hartel, M. Lampe, J. B. Aviles, Phys. Fluids 22, 2216 (1979).

19. E. P. Lee, "Model of Beam Head Erosion", Lawrence Livermore National Laboratory Report UCID-18768 (1980).

20. E. J. Lauer, R. J. Briggs, T. J. Fessenden, R. E. Hester and E. P. Lee Phys. Fluids 21, 1344 (1978); LLNL Report UCID-17840 (1978); Proceedings of the Second International Conference on High Power Electron and Ion Beam Research and Technology, Cornell Univ., p. 319 (1977).

21. J. C. Clark, T. J. Fessenden and K. W. Struve, Bull Am. Phys. Soc. 27, 1133 (1982).